ChemComm

COMMUNICATION

View Article Online
View Journal | View Issue

Cite this: *Chem. Commun.*, 2020, **56**, 6130

Received 19th February 2020,
Accepted 24th April 2020

DOI: 10.1039/d0cc01302a

rsc.li/chemcomm

Cation exchange assisted synthesis of ZnCdSe/ZnSe quantum dots with narrow emission line widths and near-unity photoluminescence quantum yields†

Xiao Jin, [ab] Kanlin Xie,[b] Tingting Zhang,[b] Huada Lian,[b] Zhenghe Zhang,[b] Bing Xu, [b] Dongyu Li[ab] and Qinghua Li *[ab]

Quantum dots with narrow emission line width have persistently received attention for their applications in biological imaging, lasers and next-generation displays. We herein report a cation exchange assisted shelling approach changing the starting CdSe emitting cores into new ZnCdSe alloy emitting cores and finally ZnCdSe/ZnSe core/shell QDs. The resulting ZnCdSe/ZnSe QDs exhibit an emission line width as narrow as 17.1 nm with a near-unity photoluminescence quantum yield and a single emission channel. We anticipate that our study on a cation exchange assisted synthetic route for controlling the emission line widths of the QDs could be extended to high-quality green and blue ones beyond currently achieved.

Quantum dots (QDs) have attracted much research interest owing to their large absorption cross section, tunable emission wavelength, pure emission colour, high photoluminescence quantum yield (PL QY) and good stability.[1] These unique properties offer a broad range of applications including solar cells, light-emitting diodes, biological imaging and next generation displays.[2–5] Quantum dots with high PL QYs and narrow emission line widths are important for realizing these potential applications and have become a long-lasting topic over the past few decades.[6] Coating an emitting core with a wider band gap material is one of the most profound discoveries for high quality quantum dots.[7] The further growth of thick shells has been proved effective to minimize the negative influence of the surface-related trap states when the shell thickness reaches a critical value (typically, >5 nm).[8] It also helps hinder the inter-dot energy transfer of the quantum dot solids by separating the emitting cores from the thick shell.[9] This is important for maintaining the optical properties of the device-grade QD solids because the inter-dot energy transfer more likely happens in a condensed state. Recent works show that the thick shell quantum dots also function well in dealing with Auger recombination and suppressing "blinking".[9–11]

Despite these prominent properties, traditional CdSe/CdS core/shell thick-shell QDs have unsatisfactory emission efficiencies, which hampers their application in LEDs. For instance, the PL QYs of the CdSe/CdS QDs decrease by over 40% as the shells grow thicker.[12,13] With the growth of the shell, the emission core suffers growing lattice strain from the shell due to the existence of the lattice mismatch of the CdSe core and the CdS shell materials. Thicker shells may generate inner defect states of the core and non-radiative recombination occurs.[14] Recent studies reveal that the structural stress can be mitigated by creating a gradient alloy interface between the core and shell materials. Klimov and his co-workers proposed a thick-shell CdS/CdSe/CdS quantum dot with a near-unity PL QY at 613 nm.[8] Later, Lei Qian synthesized 9.8 nm sized CdSe/$Cd_{1-x}Zn_xSe$/ZnSe quantum dots with a PL QY of 84% and a FWHM of 21 nm.[15] Huaibin Shen's group synthesized thick-shell CdZnSe/ZnSe/ZnS quantum dots with a PL QY $>95\%$ in solution and 90% in solids at 597 nm.[16] Their quantum dot light-emitting diodes reached the milestone external quantum efficiency (EQE) of over 30%. However, there is still much room for improving the color purity of the red emission quantum dots. All the above mentioned high quality quantum dots possess high PL QYs, but their FWHMs are 21–35 nm. Considering that the defect states have been eliminated by coating thick-shell wide band gap materials, the defect state induced broadening of emission line widths is not the main factor. The emission line widths are solely decided by the uniformity of the emitting cores. However, it still remains a challenging task to directly synthesize red emitting cores with narrow FWHMs by controlling the core synthesis conditions alone.

Unlike other work that has directly pursued emitting cores with narrow size distributions, we have developed a facile cation exchange assisted one-pot paradigm for red ZnCdSe/ZnSe simultaneously having near unity PL QYs and narrow line widths. The direct synthesis of ZnCdSe QDs by simultaneously injecting the required precursors has proven challenging because of the

[a] *Key Laboratory of Clean Energy Materials Chemistry of Guangdong Higher Education Institutes, Lingnan Normal University, Zhanjiang 524048, P. R. China. E-mail: qhli@hqu.edu.cn*

[b] *Key Laboratory of Environmentally Friendly Functional Materials and Devices, Lingnan Normal University, Zhanjiang 524048, P. R. China*

† Electronic supplementary information (ESI) available: Experimental details, and XRD patterns and TEM images of the QDs. See DOI: 10.1039/d0cc01302a

unbalanced reactivity of the commonly used $Zn(OA)_2$ and $Cd(OA)_2$ precursors.[17–19] A recently developed post-core-synthetic method has proven effective to obtain high quality ZnCdSe from the starting CdSe cores at high temperatures.[20] We herein use ZnSe to coat CdSe cores to synthesize ZnCdSe/ZnSe QDs at high temperature. The resultant ZnCdSe/ZnSe QD solution reveals a narrow emission at 631 nm with a FWHM of 17.1 nm and a PL QY of 99%. To the best of our knowledge, our ZnCdSe/ZnSe QDs have the narrowest emission line widths with near unity PL QYs around 630 nm.

Unlike those reports perusing the wide emission tunability of ZnCdSe,[17,20] we focus on the synthetic route for simultaneously achieving high PL QYs and narrow emission line widths. The basic aspects of our cation exchange based synthesis of ZnCdSe quantum dots are schematically illustrated in Fig. 1. We start with a small number of CdSe cores obtained by hot injection of a small amount of Se. With the prompt depletion of the Se by CdSe core nucleation and growth, the smaller cores dissolve while large cores grow *via* the so called Ostwald ripening, causing a size distribution broadening and a wide emission line width. Further continuous addition of Se precursor produces a ZnSe shell on the CdSe core. The core–shell structures transform into alloys rapidly, because the temperature is above the "alloying point" (above 270 °C).[20] Under these circumstances, isotropic cation exchange between the shell of Zn^{2+} and the core of Cd^{2+} occurs.[21] The slow rate of the addition of Se ensures that the cation exchange process occurs sufficiently and the CdSe/ZnSe alloys form a whole emitting ZnCdSe core. During the ZnSe shelling, the continuous supply of Se together with abundant Zn forces smaller nanocrystals to grow faster than the larger ones thereby preventing Ostwald ripening and narrowing the size distribution of the new ZnCdSe core. Although conventional shelling methods can produce monodisperse quantum dots such as CdSe/CdS,[22–25] without alloying processes, the emission line width suppression is quite limited. In this work, the existing size broadening of the emitting cores has already decided the basis of the emission regardless of how uniform the final core/shell product is. Considering the above mentioned two effects, we narrowed the FWHM of ZnCdSe/ZnSe quantum dots to 17.1 nm.

The CdSe cores were synthesized following a previously reported method with modifications.[15] In a typical core synthesis procedure, a small amount of Se stock solution (0.1 mmol) was used to produce a small number of CdSe cores. As the reaction activity of $Zn(OA)_2$ is much lower than that of $Cd(OA)_2$, Se atoms prefer to bond with Cd rather than Zn, thus forming the CdSe core.[26] As shown in Fig. S1a (ESI†), the XRD patterns of the cores show three typical peaks at 25.35°, 42.40° and 50.01°, which well match the zinc blende CdSe standard card (JCPDS 65-2891). A continuous red-shift of the diffraction patterns to larger angles with the growth of the ZnSe monolayers implies a gradual shrinkage of the unit cell lattice. This notable lattice shrinkage indicates that ZnSe tends to alloy with the CdSe core to form ZnCdSe alloys rather than undergoing pure epitaxial growth. Transmission electron microscopy (TEM) images show that the average diameter of the QDs increases with the growth of the shell (Fig. S1b–d, ESI†). Statistical results reveal that the average particle diameter of the CdSe cores is 4.6 nm with a relative standard deviation of 9.5%. The epitaxial growth of the ZnSe shell increases the average particle size to 12.5 nm and narrows the size distribution to 6%, consistent with the optical measurements. High resolution TEM images reveal that the (1 1 1) *d*-spacing decreases from 0.352 nm to 0.325 nm with the growth of ZnSe to 8 ML, implying a lattice shrinkage due to alloying. No visible stacking faults of the as-prepared ZnCdSe/ZnSe QDs suggest the good epitaxial growth of the shell.

The elemental distributions of the ZnCdSe/ZnSe (8 ML) QDs in Fig. 2a clearly show the successful growth of the ZnSe shell. The elemental mapping of a single nanocrystal shown in Fig. 2b clearly displays that the Cd elemental distribution area reaches 9.1 nm in diameter, which is much larger than that of the initial diameter of the CdSe core (4.6 nm). This larger Cd elemental distribution area indicates that Cd in the core has diffused into the shell. The Zn elemental distribution area diameter is 13.0 nm, consistent with the average size of the particles. The dark field image of the core/shell QDs also contains brighter Cd content centers and Zn element voids at the center for most dots, implying higher Cd and relatively lower Zn contents. This may relate to the gradient core/shell structure with more Cd at the center and more Zn contents in the outer shell. This type of gradient core/shell structure is known for suppressing Auger recombination and enabling high PL QYs,[27,28] which therefore well matches with the high performance of ZnCdSe/ZnSe core/shell QDs. Such a gradient

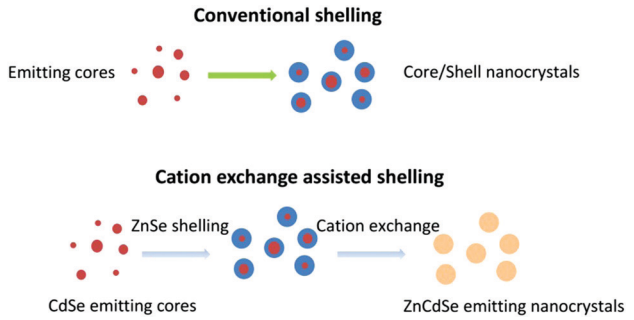

Fig. 1 Schematic illustration for conventional shelling and cation exchange assisted shelling.

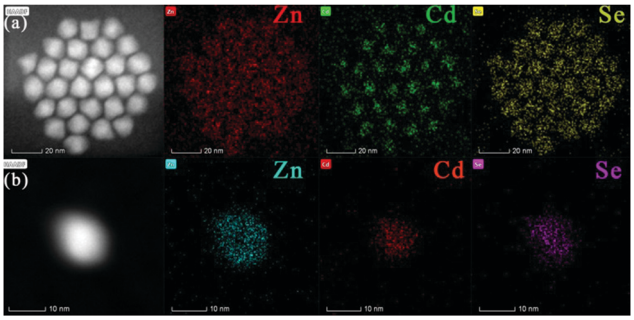

Fig. 2 (a) HAADF-STEM images of the ZnCdSe/ZnSe (8 ML) QDs. (b) Single particle HAADF-STEM images.

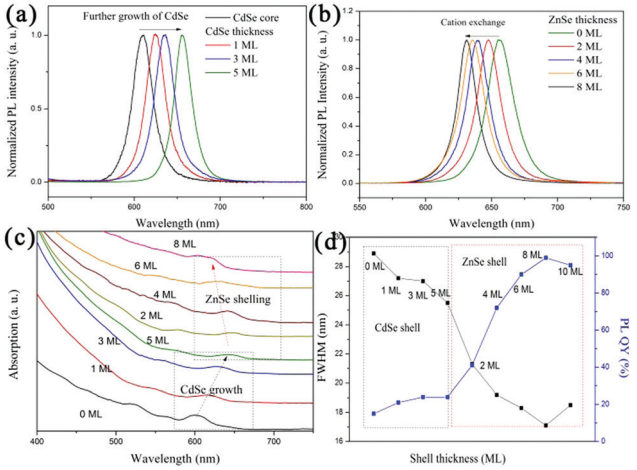

Fig. 3 (a) PL evolution illustrating the growth of the CdSe. (b) PL evolution with the ZnSe shelling. (c) Absorption spectra of the QDs with the shell growth. (d) HWHMs and PL QYs as functions of the ML number of the shells.

alloy structure with high sample uniformity could minimize inhomogeneous broadening of the emission peaks with high PL QYs.

The evolution of the absorption and PL spectra of the ZnCdSe/ZnSe/ZnS QDs during the shell growth is shown in Fig. 3a–c. Both the first exciton absorption peak and the PL peak show an obvious red shift from 609 nm to 659 nm with the initial addition of Se. Such a notable red shift is attributed to the continuous growth of the CdSe by consuming residual Cd components. However, further adding of the Se precursor leads to a notable blue shift of the emission from 659 to 631 nm. At this stage, Se bonds with Zn to form a shell and the Zn diffuses into the core to form a new alloy ZnCdSe emitting core at a high reacting temperature, thus producing a wider band gap. This significant blue shift is consistent with the alloying phenomenon from the structural analysis. Fig. 3d shows that the full width at half maximum (FWHM) of the emission is slightly compressed at the beginning of ZnSe growth but a notable narrowing with the blue shift of the PL peak. With the growth of 8 ML of ZnSe shell, the FWHM of the QDs notably decreases from 28.9 to 17.1 nm. This remarkable improvement in emission line width is ascribed to the complete alloying between the core and the ZnSe shell with the overall particle size being uniform. During the ZnSe shelling, smaller particles have higher growth rates than that of larger ones with a continuous supply of reactive monomers.[29] At the same time, the diffusion of Zn in the shell and Cd in the core occurs. Long enough reaction time guarantees that the alloying process occurs sufficiently to transform CdSe/ZnSe to a fully alloyed ZnCdSe emitter. Conventional epitaxial growth of the shell without cation exchange demonstrates huge improvements in PL quantum yields by passivating the surface of the emitting cores, but a limited role in reducing emission line widths. The size of each emitting core is not changed despite the overall diameter of core/shell QDs being uniform. The epitaxy of the first several MLs of ZnSe leads to a PL QY boost,

Table 1 Comparison of FWHMs and PL QYs with the existing best red emitting QDs

QDs	Wavelength (nm)	FWHM (nm)	PL QY (%)	Ref.
CdSe/CdS	580	21	97	6
CdSe/$Cd_{1-x}Zn_xSe$/ZnSe	630	21	84	15
$Zn_{1-x}Cd_xSe$/ZnSe/ZnS	597	25	95	30
CdS/CdSe/CdS	613	35	99	8
ZnCdSe/ZnSe	631	17.1	99	This work

owing to the passivation effect of ZnSe by dealing with the dangling bonds on the surface (Fig. 3d). The PL QY of the ZnCdSe/ZnSe QDs increases steadily to near unity upon shell ZnSe epitaxy to 8 MLs. The growth of ZnSe exceeding 8 MLs may produce lattice strain induced defect states that decrease the PL QY. We compared the optical properties of our ZnCdSe/ZnSe QDs with those reported in the literature (Table 1). Our QDs exhibit the narrowest FWHM of 17.1 nm with a near unity PL QY.

In order to identify the effect of the ZnSe shell on passivating the defect states of the emitting cores, time-resolved PL (tr-PL) tests were performed. The tr-PL decay of the ZnCdSe core displays a fast decay within 2 ns, a moderate decay below 10 ns and a long decay tail (Fig. 4a). Previous study has demonstrated that the hole traps associated with unbounded Se sites are nearly not emissive with a fast decay channel.[31] The moderate decay term is the intrinsic radiative recombination. The long decay tail is related to the shallow electron traps originating from either excess cadmium carboxylate or the removal of fatty ligands.[9,31] Therefore, a three-exponential function is able to fit the curve.

The theoretical curve fits well with the tr-PL data of CdSe and the chi-square goodness-of-fit χ_R^2 is 0.68 (Table S1, ESI†), indicating that our theoretical calculation model has high reliability.[23] For ZnCdSe/ZnSe (2 ML) QDs, the fast decay term is greatly suppressed (Fig. 4b). The overall tr-PL curve shows a

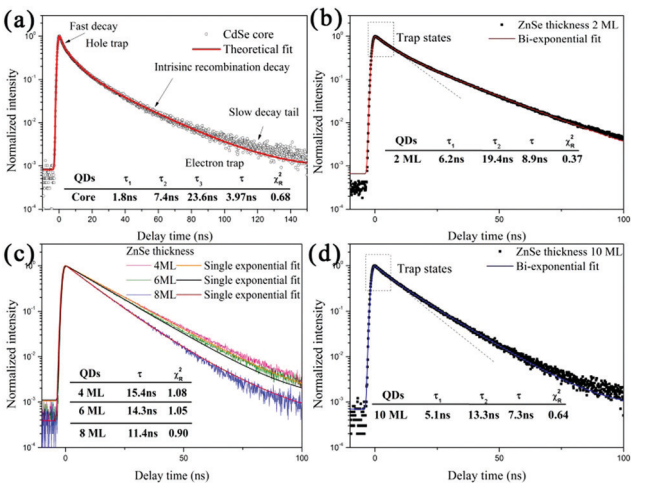

Fig. 4 Tr-PL decay curves and theoretical fitted lines of the CdSe cores (a), ZnCdSe/ZnSe (2 ML) (b), ZnCdSe/ZnSe (4, 6, and 8 ML) (c) and ZnCdSe/ZnSe (10 ML) (d).

much double-channel like decay with χ_R^2 = 0.37 by bi-exponential fitting. The average lifetime of the QDs with 2 ML ZnSe (8.9 ns) is 2 times longer than that of the cores, suggesting the reduction of hole trap states. Further growth of the ZnSe shell (4–8 ML) results in a much single-channel like decay with a nonvisible fast decay component (hole traps) (Fig. 4c). Growth of the 8 ML ZnSe shell leads to a nearly 100% PL QY with a perfect single exponential PL decay curve, with the smallest best χ_R^2 of 0.90 by single exponential fitting, implying the good passivation and isolation of the electron traps from the thick shell. Besides, the average PL lifetimes show a clear decrease with an increase in the ZnSe shell from 4–10 MLs. Such a notable decease of the PL lifetimes suggests an enhanced stimulated radiation recombination probability, which is consistent with the related ZnCdSe/ZnS system.[9] As a wide band gap material, a thicker ZnSe shell increases restrictions on electron holes in the ZnCdSe core, enhances the stimulated radiation recombination probability and decreases the PL lifetime. However, the trap states emerge as the ZnSe shell exceeds 8 ML (Fig. 4d), leading to a decrease in the PL QY.

In summary, we proposed a cation exchange assisted approach for fabricating ZnCdSe/ZnSe core/shell alloy QDs. The as-prepared ZnCdSe/ZnSe (8 ML) QDs exhibit an extremely narrow emission line width (17.1 nm). The alloying process occurs during the ZnSe shelling, which causes the starting CdSe cores to alloy into ZnCdSe emitting cores. As the smaller cores grow faster than the larger ones, the monodispersity of the new born ZnCdSe emitting cores is improved, leading to a remarkable suppression in PL emission line width. Tr-PL results reveal that both the hole trap states from the Se dangling bonds and shallow electron trap states from cation dangling bonds diminish as the shell growth exceeds 4 MLs. As a result, the ZnCdSe/ZnSe (8 ML) QDs reach a PL QY as high as 99%. Our study provides a new platform to adjust the emission line width through cation assisted shelling without sophisticated synthetic routes for controlling the nucleation.

We gratefully acknowledge the financial support from the Natural Science Foundation of China (11774141), the Natural Science Foundation of Guangdong Province (2019A1515011228, 2019A1515011461, and 2018A030307011), the Innovation Team of Guangdong Higher Education Institutes (2019KCXTD012) and the Natural Science Foundation of Jiangxi Province (20192ACBL21045).

Conflicts of interest

The authors declare no competing financial interest.

Notes and references

1 M. V. Kovalenko, L. Manna, A. Cabot, Z. Hens, D. V. Talapin, C. R. Kagan, V. I. Klimov, A. L. Rogach, P. Reiss, D. J. Milliron, P. Guyot-Sionnnest, G. Konstantatos, W. J. Parak, T. Hyeon, B. A. Korgel, C. B. Murray and W. Heiss, *ACS Nano*, 2015, **9**, 1012–1057.
2 H. Shen, Q. Gao, Y. Zhang, Y. Lin, Q. Lin, Z. Li, L. Chen, Z. Zeng, X. Li, Y. Jia, S. Wang, Z. Du, L. S. Li and Z. Zhang, *Nat. Photonics*, 2019, **13**, 192–197.
3 C.-H. M. Chuang, P. R. Brown, V. Bulović and M. G. Bawendi, *Nat. Mater.*, 2014, **13**, 796–801.
4 Z. Pan, I. Mora-Seró, Q. Shen, H. Zhang, Y. Li, K. Zhao, J. Wang, X. Zhong and J. Bisquert, *J. Am. Chem. Soc.*, 2014, **136**, 9203–9210.
5 D. Franke, D. K. Harris, O. Chen, O. T. Bruns, J. A. Carr, M. W. B. Wilson and M. G. Bawendi, *Nat. Commun.*, 2016, **7**, 12749.
6 O. Chen, J. Zhao, V. P. Chauhan, J. Cui, C. Wong, D. K. Harris, H. Wei, H.-S. Han, D. Fukumura, R. K. Jain and M. G. Bawendi, *Nat. Mater.*, 2013, **12**, 445.
7 X. Peng, M. C. Schlamp, A. V. Kadavanich and A. P. Alivisatos, *J. Am. Chem. Soc.*, 1997, **119**, 7019–7029.
8 B. G. Jeong, Y.-S. Park, J. H. Chang, I. Cho, J. K. Kim, H. Kim, K. Char, J. Cho, V. I. Klimov, P. Park, D. C. Lee and W. K. Bae, *ACS Nano*, 2016, **10**, 9297–9305.
9 Z. Li, F. Chen, L. Wang, H. Shen, L. Guo, Y. Kuang, H. Wang, N. Li and L. S. Li, *Chem. Mater.*, 2018, **30**, 3668–3676.
10 A. L. Efros and D. J. Nesbitt, *Nat. Nanotechnol.*, 2016, **11**, 661–671.
11 Y.-S. Park, J. Lim and V. I. Klimov, *Nat. Mater.*, 2019, **18**, 249–255.
12 W. K. Bae, L. A. Padilha, Y.-S. Park, H. McDaniel, I. Robel, J. M. Pietryga and V. I. Klimov, *ACS Nano*, 2013, **7**, 3411–3419.
13 B. N. Pal, Y. Ghosh, S. Brovelli, R. Laocharoensuk, V. I. Klimov, J. A. Hollingsworth and H. Htoon, *Nano Lett.*, 2012, **12**, 331–336.
14 K. Gong and D. F. Kelley, *J. Phys. Chem. Lett.*, 2015, **6**, 1559–1562.
15 W. Cao, C. Xiang, Y. Yang, Q. Chen, L. Chen, X. Yan and L. Qian, *Nat. Commun.*, 2018, **9**, 2608.
16 J. Song, O. Wang, H. Shen, Q. Lin, Z. Li, L. Wang, X. Zhang and L. S. Li, *Adv. Funct. Mater.*, 2019, **29**, 1808377.
17 Y. Yuan, H. Zhu, X. Wang, D. Cui, Z. Gao, D. Su, J. Zhao and O. Chen, *Chem. Mater.*, 2019, **31**, 2635–2643.
18 S. Lee, D.-E. Yoon, D. Kim, D. J. Shin, B. G. Jeong, D. Lee, J. Lim, W. K. Bae, H.-K. Lim and D. C. Lee, *Nanoscale*, 2019, **11**, 15072–15082.
19 O. Yarema, M. Yarema and V. Wood, *Chem. Mater.*, 2018, **30**, 1446–1461.
20 X. Zhong, M. Han, Z. Dong, T. J. White and W. Knoll, *J. Am. Chem. Soc.*, 2003, **125**, 8589–8594.
21 E. Groeneveld, L. Witteman, M. Lefferts, X. Ke, S. Bals, G. Van Tendeloo and C. de Mello Donega, *ACS Nano*, 2013, **7**, 7913–7930.
22 H. Qin, Y. Niu, R. Meng, X. Lin, R. Lai, W. Fang and X. Peng, *J. Am. Chem. Soc.*, 2014, **136**, 179–187.
23 J. Zhou, M. Zhu, R. Meng, H. Qin and X. Peng, *J. Am. Chem. Soc.*, 2017, **139**, 16556–16567.
24 J. Zhou, C. Pu, T. Jiao, X. Hou and X. Peng, *J. Am. Chem. Soc.*, 2016, **138**, 6475–6483.
25 Y. Wang, C. Pu, H. Lei, H. Qin and X. Peng, *J. Am. Chem. Soc.*, 2019, **141**, 17617–17628.
26 H. Cao, J. Ma, L. Huang, H. Qin, R. Meng, Y. Li and X. Peng, *J. Am. Chem. Soc.*, 2016, **138**, 15727–15735.
27 J. Lim, Y.-S. Park and V. I. Klimov, *Nat. Mater.*, 2018, **17**, 42–49.
28 J. Lim, B. G. Jeong, M. Park, J. K. Kim, J. M. Pietryga, Y.-S. Park, V. I. Klimov, C. Lee, D. C. Lee and W. K. Bae, *Adv. Mater.*, 2014, **26**, 8034–8040.
29 M. D. Clark, S. K. Kumar, J. S. Owen and E. M. Chan, *Nano Lett.*, 2011, **11**, 1976–1980.
30 J. Song, O. Wang, H. Shen, Q. Lin, Z. Li, L. Wang, X. Zhang and L. S. Li, *Adv. Funct. Mater.*, 2019, **29**, 1808377.
31 Y. Gao and X. Peng, *J. Am. Chem. Soc.*, 2015, **137**, 4230–4235.